Flexural Strengthening of RC Beams Using Steel Reinforced Polymer (SRP) Composites

by Y.J. Kim, A. Fam, A. Kong, and R. El-Hacha

Synopsis: This paper presents the application of a new generation of externally bonded composite material in flexural strengthening of reinforced concrete beams. The steel reinforced polymer (SRP) composite consists of high-carbon steel unidirectional Hardwire® fabrics embedded in epoxy resin, and offers high strength and stiffness characteristics at a reasonable cost. In this paper, the mechanical properties of SRP are evaluated and its application in flexural strengthening of RC beams is investigated. Six beams have been tested in three-point bending to study the effect of SRP retrofitting on flexural behavior, failure modes, and crack patterns. Test parameters include variation of the width of SRP sheets and the use of SRP U-wraps to prevent premature failure caused by delamination of the longitudinal sheet. Significant increase in flexural capacity, up to 53%, and pseudo-ductile failure modes were observed in SRP-strengthened beams. Failure was governed primarily by concrete cover delamination at the ends of SRP sheets or concrete crushing. The U-wraps improved flexural stiffness by means of controlling diagonal cracking and providing anchorages to the longitudinal SRP sheets, which reduced their slip. Shear stress concentrations near cut-off points of SRP sheets have also been investigated. An analytical model was used to predict the nominal flexural strength of SRP-strengthened beams.

1648 Kim et al.

ACI Member **Yail J. Kim** is a Ph.D. Candidate at Queen's University, Kingston, Canada. He obtained his B.Eng. from Dongguk University, Seoul, Korea in 1994 and M.A.Sc. from the University of Windsor, Windsor, Canada in 2002. He is an associate member of ACI-440. His research interests include strengthening deteriorated structures using advanced composite materials based on computational mechanics and fracture mechanics

ACI Member **Amir Fam** is an Assistant Professor and Canada Research Chair in Innovative and Retrofitted Structures at Queen's University, Canada. He is a voting member of ACI Committee 440, Fiber Reinforced Polymer (FRP) Reinforcement, and co-chair of Sub-Committee 440-J, FRP Stay-in-Place Formwork. His research interests include applications of FRPs in new construction and retrofit of existing structures.

Andrew Kong is a Masters Student in the Department of Civil Engineering at Queen's University at Kingston, Ontario, Canada. He received a B.Sc. from North Carolina A&T State University, U.S.A., 2002. Current research involves durability of fiber reinforced polymers used as external reinforcement of concrete cylinders.

ACI Member **Raafat El-Hacha** is an Assistant Professor in the Department of Civil Engineering at the University of Calgary, Canada. He is a voting member of ACI Committee 440, Fiber Reinforced Polymer (FRP) Reinforcement, and co-chair of Sub-Committee 440-I, FRP Prestressed Concrete. His research interests include strengthening, reinforcing and prestressing concrete structures with FRPs.

INTRODUCTION

Various rehabilitation techniques have been proposed for civil infrastructure to overcome problems associated with the aging process, increased traffic, change in use, and deterioration. Among these techniques, external strengthening provides a practical and cost effective solution when compared to other traditional repair methods. The first generation of external strengthening methods utilized steel plates bonded to the tension surface of the structure. The strengthening effectiveness was acceptable; however several problems, including durability, heavy weight, handling, and shoring, had to be resolved; thus the need for alternative materials aroused. The introduction of advanced composite materials, particularly fiber reinforced polymers (FRPs), in structural engineering industries, as a second generation of externally bonded retrofit materials, has offered numerous benefits (i.e. corrosion-free, excellent weight to strength ratio, good fatigue resistance, flexibility to conform to any shape, and broad applications). Retrofit of structures using glass-FRP (GFRP) and carbon-FRP (CFRP) has been studied extensively over the past decade (Meier 1995; Neale 2000; Bakis et al. 2002 among many others). Although the applications of FRPs are becoming wider and popular, the cost of material is still relatively high. Recently, a new composite material has been developed to overcome this shortcoming. The steel reinforced polymer (SRP) consists of high-carbon steel unidirectional Hardwire® fabrics embedded in polymer matrix. Each cord comprising the fabrics has a somewhat similar appearance to conventional prestressing strands, but at a much smaller scale (i.e. approximately 0.9 mm diameter each). Another advantage of SRP, although not investigated in this study, is the ability to bend around

90° corners of minimum radius of curvature, without significant reduction in strength due to stress concentration. The installation process of SRP is quite similar to that of other conventional FRP materials. The unidirectional Hardwire® fabrics are impregnated with resin during installation to a prepared concrete surface; then adequately cured. To date, one study has been reported on retrofit of concrete beams using SRP (Wobbe et al. 2004), where different bonding agents and different number of plies were investigated.

RESEARCH SIGNIFICANCE

This paper reports the test results of an experimental investigation carried out on reinforced concrete beams strengthened in flexure using steel reinforced polymer (SRP). SRP is an emerging new composite that offers mechanical properties comparable to those of CFRP at a reduced cost. The study investigates the effect of reinforcement ratios of SRP, in terms of the width of the sheet attached to the tension face of the beam as well as the effect of using SRP U-wraps for the anchorage of longitudinal SRP sheets. This study is also focused on examining the shear stress concentrations near the cut-off points of SRP, as well as evaluating the contribution of SRP U-wraps to flexural stiffness through diagonal crack control and slip control of the longitudinal SRP sheet.

EXPERIMENTAL PROGRAM

Beam Details and Instrumentation

Six simply supported rectangular reinforced concrete (RC) beams of 100 x 150 mm cross-section and 1,220 mm long were tested in three-point bending to evaluate the flexural behavior of SRP-strengthened RC beams. All beams were reinforced with two No. 10 M bars (A_s = 100 mm^2 each) and had an effective depth of 130 mm. The beams were adequately reinforced for shear using plain bars 6 mm diameter two-leg steel stirrups, placed at 100 mm spacing. The test specimens included one control beam, designated (control), four beams strengthened using SRP sheets of three different widths, namely 30, 60, and 100 mm (i.e. SRP 30, SRP 60, SRP 100-1, and SRP 100-2), where specimens SRP 100-1 and -2 were identical. One additional beam was strengthened using a 100 mm wide SRP sheet, anchored at both ends using 150 mm wide SRP U-wraps. Fig. 1 shows the typical beam details for different SRP configurations, including instrumentation and test set-up.

Two linear variable displacement transducers (LVDTs) were used to monitor the mid-span deflection and crack mouth opening displacement. Two displacement-type strain gauge transducers (PI-gauges) were installed on the compression and tension sides at mid-span of the beams, where the tension PI-gauge was located at the same elevation of the internal reinforcement. Electrical resistance strain gauges were installed at various locations on the SRP sheets to establish the strain distribution along the length of SRP sheet under increased loads, particularly near the critical zones at the ends of the SRP sheets, as shown in Fig. 1 (b). A 50,000 lb (222 kN) capacity load-cell was used at the loading point.

Materials

Steel Reinforced Polymer (SRP) -- The SRP consisted of twisted high-carbon steel cords (Hardwire[®] 3x2-23-12) embedded into a polymeric resin (Sikadur[®] 330). Each steel cord is coated with a micro-fine brass or AO-brass (Adhesion Optimized), and consists of three straight steel wires surrounded by two wires wrapped at a high twist angle. According to the manufacturer (Hardwire LLC 2004), each steel cord has a diameter of 0.89 mm and the composite laminate thickness is 1.2 mm.

The epoxy resin consists of Components A and B, which are mixed at a ratio of 4:1 by weight and stirred until a homogenous mixture is obtained. The resin has a tensile strength of 30 MPa, a flexural modulus of 3.8 GPa, and an ultimate elongation of 1.5 % (Sika Corp. 2004). It is suggested by the manufacturer that the volumetric steel wire to resin ratio of SRP should be 1: 1.7.

Three composite SRP coupons (25 mm x 250 mm), prepared in accordance to ASTM D 3039-00 (ASTM 2000), were tested using a MTS testing machine with hydraulic grips, as shown in Fig. 2 (a). All coupons were instrumented with two electric resistance strain gauges in the longitudinal and transverse directions. The applied loads, corresponding strokes, and strain gauge readings were recorded using a data acquisition system. The measured mechanical properties of the SRP coupons are summarized and compared with the manufacturer's data in Table 1. A picture of the failed specimens is shown in Fig. 2 (b). Unlike GFRP and CFRP materials, the SRP showed a somewhat nonlinear stress-strain response, as shown in Fig. 2 (c).

Concrete and Steel Reinforcement -- The 28 day specified concrete strength was 39.4 MPa and the concrete strength at the time of beam testing was 46.2 MPa. The flexural steel reinforcement of test beams had yield strength of 472 MPa with a standard deviation of 25 MPa, and an ultimate strength of 621 MPa with a standard deviation of 38 MPa, based on tension tests.

Fabrication of Test Specimens

In order to guarantee adequate bond between the concrete surface and SRP, the tension faces of all beams were sandblasted until coarse aggregates were exposed and all laitance, dust, and dirt were removed using air pressure. A layer of the epoxy resin was applied uniformly on the tension surface of the beam; then unidirectional Hardwire[®] fabrics were placed and pressed into the resin, and an additional layer of resin was applied to completely cover the cords. A typical application procedure of the SRP sheet is shown in Fig. 3. Care was taken to control a uniform thickness of the epoxy-SRP composites. The minimum curing time of SRP was seven days at room temperature.

Test Set-up and Procedure

Beam specimens were tested in three-point bending over a 1,110 mm span, using a 900 kN Riehle testing machine, as shown in Fig. 1 (a). The load was applied using stroke control at a 1 mm/min rate of loading. Steel plates, 75 mm wide, were positioned at the supports and a 20 mm wide plate was positioned at the loading point to distribute the loads and to avoid local crushing of concrete. To investigate the crack mouth opening

displacement (CMOD), all beams were first loaded to about 10 kN until initial visual cracks were observed; then were completely unloaded to install a horizontal LVDT near mid-span, where the largest crack opening was visually observed. The corresponding residual deflections after unloading were recorded. The unloaded beams were then monotonically reloaded to failure.

EXPERIMENTAL RESULTS

Behavior of Test Beams and Effect of Different Parameters

The load-deflection responses of the six beam specimens are shown in Fig. 4. Initial cracks in all beams were observed near mid-span at low load levels, between 5 kN and 15 kN. The ultimate load capacities of specimens SRP 30, SRP 60, SRP 100, and SRP U100 were increased by 18 %, 34 %, 32 %, and 53 %, respectively, with respect to the control specimen. It is also noted that the stiffness of test beams slightly increased as the width of SRP sheet increased, particularly for specimen SRP U100, as will be discussed later. Table 2 shows a summary of test results of the beams, in terms of load and deflections at cracking, yielding, and ultimate stages as well as the strain measurements. For SRP-strengthened beams, a concrete crushing failure, after yielding of the internal reinforcement, was desired rather than delamination of the longitudinal sheets; however delamination preceded crushing in some beams (i.e. SRP 100-1 and SRP 100-2). The effect of delamination of the SRP sheets can be observed in Fig. 4, where a sudden load drop occurred. Delamination in the form of the peeling-off failure mode occurred within the concrete cover as a result of the excessive stress concentrations induced by normal and shear stresses at the end of the SRP sheet. After complete delamination of SRP sheet, the load dropped to a level equivalent to or slightly lower than that of the control beam. This is attributed to the impact caused at failure and the excessive damage caused in the strengthened beams, compared to the control beam, at a load level higher than the yielding load of the control beam. However, as loading continued, the load was slightly recovered in some of the beams and approached that of the control specimen.

Beams SRP 100-1 and -2 showed some reduction of stiffness at a load of about 40 kN before a sudden and complete delamination occurred at 59 kN. The reduced stiffness is attributed to the development of diagonal cracks within the shear spans, which contributed to additional deflections of the beams. Another possible factor that influenced the reduced stiffness is the shear deformation of the resin at the interface between the concrete substrate and the SRP sheets. This, in fact, is supported by comparing the behavior of SRP 100-1 and -2 to that of SRP U100, which showed higher stiffness than SRP 100-1 and -2, until crushing of concrete occurred, without any significant stiffness degradation. This suggests that the U-wraps not only have effectively restrained the diagonal crack opening by acting as shear reinforcement, which reduced mid-span deflection, but also restrained the horizontal shear deformations of the interface resin.

Fig. 5 (a) shows the load versus strain measured at mid-span on the SRP sheets. Fig. 5 (b) shows a typical variation of strains along the length of the SRP sheet in specimen SRP 100, at various load levels. It is noted that the maximum strain measured was 3,143 micro-strains, which is well below the ultimate strain of SRP (see Fig. 2(c)). This is due

to the delamination failure mode of SRP, which initiated at the cut-off points and occurred before rupture of the sheets.

Failure Modes and Crack Patterns

The principal failure mode of the strengthened beams, except for SRP U100, occurred due to either SRP delamination or crushing of concrete after yielding of the internal reinforcement. Crushing of concrete occurred shortly after delamination in the case of SRP 100-1 and -2; however, other beams exhibited the opposite sequence. The delamination within the concrete cover occurred due to the high normal and shear stress concentrations at the end of the SRP sheet. Initially, horizontal cracks developed due to the stress concentrations at the cut-off point of the SRP sheet, and propagated along the level of the internal reinforcement, towards mid-span. Delamination occurred at the level of steel rebar, as shown in Fig. 6(a), due to the relatively less concrete cross sectional area at this level, which fails to maintain the interfacial shear and normal stresses. After delamination, the load dropped and flexural behavior of the strengthened beams became similar to that of the unstrengthened beam. The SRP sheet of SRP U100 slipped within the U-wraps, as shown in Fig. 6(b), rather than having clear delamination, and a sudden drop of load occurred at a load of 68 kN. Beams SRP 60 and SRP 30 showed similar behavior to the SRP 100 beams; however, the impact of delamination was relatively lower, due to the smaller size of SRP sheets, and hence the lower tension forces. The prevention of the concrete cover delamination, which governs the ultimate strength of strengthened beams, is critical. ACI 440.2R-02 suggests adequate cut-off points of the external reinforcement and the use of U-wraps, as follows: the external reinforcement should extend a distance, equal to the effective depth of the beam from the point where the applied moment is equal to the cracking moment. Additional confining reinforcement such as U-wraps is also necessary if the applied shear force is higher than 2/3 the shear resistance provided by concrete (i.e. $V_u \geq 2/3$ V_c). These recommendations were implemented in design of the test specimens in the current experimental program (i.e. the SRP series and SRP U100); therefore the ultimate loads of the tested beams were very close to the theoretically predicted loads, as shown in Table 2, which is discussed later. All beams showed a ductile response due to the excessive yielding of the internal reinforcement. It is worth noting that, unlike non-U-wrapped beams which showed fewer cracks, in the U-wrapped beam (i.e. SRP U100) several small cracks were formed and were spread along the span, as shown in Fig. 6(c). These effectively-distributed small cracks are somewhat similar to those observed in beams strengthened with prestressed CFRP sheets (El-Hacha et al. 2004). This observation supports the hypothesis that the U-wraps have efficiently constrained the horizontal slip of the SRP sheet, which has resulted in better bonding conditions and anchorage at the ends. This behavior also explains the stiffer behavior of the U-wrapped beam, shown in Fig. 4.

Crack Mouth Opening Displacements

As the externally applied load increased beyond the initial cracking load of the beams, the crack depth and crack mouth opening displacement (CMOD) also increased. Fig. 7 shows the comparison of the CMODs of the tested beams. Initially, the CMOD increased almost linearly. CMODs significantly influence durability of structures and may accelerate corrosion of the internal reinforcement by permitting more moisture

migrations. Most building codes suggest crack control in terms of crack width control or indirect crack control parameters (CSA A23.3-94 and CSA S806-02). The recommended values are 0.33 mm to 0.4 mm at service loads, depending on the environmental conditions (i.e. internal or external exposures). As shown in Fig. 7, most of the beams satisfied the suggested range at loads within the service load levels (i.e. typically 60% of the yield load). It should also be noted that randomness of crack occurrence might affect the CMOD. For example, CMOD of SRP 30 was greater than that of the control specimen, initially. Similarly, CMOD of SRP U100 was greater than that of SRP 100.

ANALYTICAL MODEL

A simple analytical model is proposed to predict the nominal strength of the SRP-strengthened beams, using force equilibrium and strain compatibility and is based on concrete crushing failure prior to SRP delamination. The following simplifying assumptions are made in the model: plane sections remain plane, no strain-lag effects influence on flexural behavior (i.e. shear slip of the resin is not accounted for), the ultimate strain of concrete (ε_{cu}) is 0.0035, micro damage and nonlinearity in SRP are not accounted for, perfect bond between materials is assumed up to failure, and the internal steel reinforcement behaves as an elastic-perfectly-plastic material. The equation for nominal moment is given as follows:

$$M_n = f_y A_s (d - a/2) + E_{SRP} \frac{\varepsilon_{cu}(\beta_1 h - a)}{a} t_{SRP} w_{SRP} (h - a/2) \tag{1}$$

where, M_n is the nominal moment that the beam can sustain; f_y and A_s are the yield strength and cross sectional area of rebar; d, a, β_1, and h are the effective depth, depth of equivalent rectangular concrete stress block (obtained using force equilibrium), coefficient of the concrete stress block (β_1= 0.97-0.0025f'$_c$: CSA A23.3-94) and total depth of the beam, respectively; E_{SRP}, t_{SRP}, and w_{SRP} are the elastic modulus, thickness, and width of SRP, respectively. Measured material properties were used in Eq. (1). Deflection of test beams was also predicted using the effective moment of inertia method (i.e. Branson Equation) (ACI 318-02), where the transformed section properties, accounting for SRP sheets and rebar were considered. Fig. 8 shows a plot of the nominal moments predicted using Eq. 1 versus the width of SRP sheets. Also shown in the same figure are the experimental values for the test specimens. Good agreement is observed and the small differences between the analytical and experimental results could be attributed to the slip of the resin and the premature failure due to delamination of the sheet (for specimens SRP 100). The flexural strength of test specimens was also predicted using the ACI 440.2R-02 design guide. The predicted moments are shown in Fig. 8 and agree well with the experimental results and Eq. 1. The predicted loads using Eq. 1 and deflections of test beams are also given in Table 2. It is noted that the theoretical deflections were underestimated since the shear deformation due to diagonal cracking have resulted in increasing the mid-span deflections. The contribution of shear deformation is not accounted for in the ACI 318-02 equation. Specimen SRP 60, strengthened using a 60 mm wide SRP sheet, achieved almost 90 % of the ultimate load of beams SRP 100-1 and -2, with a 100 mm SRP width. Also, the ultimate load of SRP

60 was very close to the theoretical value, based on compression failure and full composite action. This indicates that SRP 60 has reached its full potential strength before delamination occurred. As such, this width of SRP sheet may be considered optimum in this case.

The average horizontal shear stress distribution was also calculated using Eq. 2 at the interface between the concrete and SRP sheet, based on the experimental tensile strains measured along the length of SRP sheet, at various load levels as shown in Fig. 9.

$$\tau_{average}(x) = \frac{\Delta\varepsilon_{SRP}(x)E_{SRP}t_{SRP}}{\Delta L} \tag{2}$$

where, $\tau_{SRP}(x)$, $\Delta\varepsilon_{SRP}$, and ΔL are the average calculated shear stress, measured tensile strain difference between two locations in SRP, and the distance between the two locations. A theoretical shear stress value calculated using classical beam theory, as given by Eq. 3, is also shown in Fig. 9. The theoretical beam theory model predicted the shear stress well, except for the near-ends of the SRP sheet, where high stress concentrations and sudden increase in shear stresses occurred and caused delamination of the sheet, as shown by the experimental values, obtained using Eq. 2.

$$\tau(x) = \frac{VQ}{Ib} \tag{3}$$

where, $\tau(x)$, V, Q, I, and b are the shear stress, shear force, first moment of area, inertia, and width of the beam.

SUMMARY AND CONCLUSIONS

This study has addressed the use of a new composite material, namely steel reinforced polymer (SRP), in flexural strengthening of rectangular reinforced concrete beams. Material characteristics of SRP have been established using coupon tests. Six beam specimens were tested using SRP sheets of various widths as well as a control specimen. The use of SRP U-wraps as end anchorage for the longitudinal SRP sheet has also been investigated. The following conclusions are drawn:

(1)   Significant increase in flexural strength, up to 53 %, was achieved in the beams strengthened with SRP sheets. Except for the beam with 100 mm wide SRP sheet, all other beams failed in compression by concrete crushing, followed by the concrete cover delamination induced by high stress concentrations at the cut-off point of the SRP sheet. The beam strengthened with a 60 mm wide SRP sheet achieved 90 % of the moment capacity of the beam strengthened with a 100 mm SRP sheet that failed by delamination before concrete crushing.

(2)   Additional transverse reinforcement such as U-wraps could delay the premature peeling-off failure of the SRP sheet by providing end anchorage. The confining effect of U-wraps reduced the slip of longitudinal SRP sheet that resulted from shear deformation

of the resin at the interface between the concrete and SRP sheet. Additionally, U-wraps reduce shear deformations induced by diagonal cracking of concrete.

(3) The proposed theoretical model is simple and has successfully predicted the ultimate loads of the test beams. The shear stress model based on the classical beam theory exhibited good agreement with test results except in the vicinity of the cut-off points of the sheet where high shear stress concentrations occurred.

ACKNOWLEDGMENTS

REFERENCES

ACI Committee 318, "Building Code requirements for Structural Concrete (ACI 318-02) and Commentary (ACI 318R-02)," American Concrete Institute, Farmington Hills, MI, USA, 443 pp.

ACI Committee 440, 2002, "Guide for the Design and Construction of Externally Bonded FRP Systems for Strengthening Concrete Structures (440.2R-02)," American Concrete Institute, Farmington Hills, MI, USA, 41 pp.

ASTM D 3039-00, 2000, "Standard Test Method for Tensile Properties of Polymer Matrix Composite Materials," ASTM International, West Conshohohoken, PA, USA, pp. 99-109.

Bakis, C.E.; Bank, L.C.; Brown, V.L.; Cosenza, E.; Davalos, J.F.; Lesko, J.J.; Machida, A.; Rizkalla, S.H.; and Triantafillou, T.C., 2002, "Fiber-Reinforced Polymer Composites for Construction-State-of-the-Art Review," *Journal of Composites for Construction*, ASCE, Reston, VA, USA, V. 6, N. 2, 2002, pp. 73-87.

CSA A23.3-94, "Concrete Design Handbook, CSA Standard A 23.3-94: Design of Concrete Structures," 2nd edition, Canadian Portland Cement Association, Ottawa, ON, Canada, 1995, 220 pp.

CSA S806-02, 2002, "Design and Construction of Building Components with Fibre-Reinforced Polymers," Canadian Standard Association, Toronto, ON, Canada, 177 pp.

El-Hacha, R.; Wight, R.G.; and Green, M.F., 2004, "Prestressed Carbon Fiber Reinforced Polymer Sheets for Strengthening Concrete Beams at Room and Low Temperatures," Journal of Composites for Construction, ASCE, Reston, VA, USA, V. 8, No. 1, 2004, pp. 3-13.

1656 Kim et al.

Hardwire LLC, 2004 "3X2 Cord and Tape Specification Sheet," Hardwire LLC, Pocomoke City, MD, USA, http://www.hardwirellc.com/Downloads/3X2_Cord_US.pdf.

Meier, U., 1995, "Strengthening of Structures Using Carbon Fibre/Epoxy Composites," Construction and Building Materials, Elservier Science Publishers Ltd., London, UK, V. 9, N. 6, 1995, pp. 341-351.

Neale, K.W., 2000, "FRPs for Structural Rehabilitation: a Survey of Recent Progress," Progress in Structural Engineering and Materials Journal, John Wiley & Sons Ltd., Hoboken, NJ, USA, V. 2, 2000, pp. 133-138.

Sika Corporation, "Sikadur® High-modulus, high-strength, impregnating resin," Sika Corp. Lyndhurst, NJ, 2004, http://www.sikaconstruction.com/tds-cpd-Sikadur330-us.pdf.

Wobbe, E.; Silva, P.; Barton, B.L.; Dharani, L.R., Birman, V.; Nanni, A.; Alkhrdaji, T.; Thomas, T.; and Tunis, G., 2004, "Flexural Capacities of RC Beams Externally Bonded with SRP and SRG," http://www.hardwirellc.com/Downloads/Flex_Capacity.pdf, 8. pp.

Table 1 — Material properties of SRP

	Elastic modulus (GPa)		Tensile strength (MPa)		Poisson's ratio		Rupture strain (%)	
	E	S[2]	σ	S[2]	μ	S[2]	ε	S[2]
Manufacturer [1]	77.9	-	1,171	-	-	-	-	-
Coupon tests	80.2	4.5	1,137	65	0.32	0.03	1.87	0.06

[1] Hardwire® (Hardwire LLC, 2004); [2] standard deviation

Table 2 — Summary of test results of beam specimens: units – Load (kN),
Deflection (mm), Mid-strain (micro-strain)

		At cracking		At yielding [1]			At ultimate		
		Exp.	Theo.	Exp.	Theo.	Mid-strain (Exp) [3]	Exp	Theo.	Mid-strain (Exp) [3]
Control	Load	5.34	6.27	42.65	36.36	-	45.05	40.35	-
	Defl.	0.34	0.17^2	5.05	2.39^2		8.10	N/A^5	
SRP 30	Load	6.43	6.37	35.12	37.89	2176	53.01	51.95	5148
	Defl.	0.36	0.17^2	3.47	2.48^2		8.47	N/A^5	
SRP 60	Load	6.65	6.48	50.39	41.06	3020	60.32	59.18	3999
	Defl.	0.39	0.17^2	6.01	2.57^2		8.61	N/A^5	
SRP 100-1	Load	9.27	6.59	53.34	46.33	2890	59.23	66.11	3143
	Defl.	0.57	0.17^2	5.10	2.68^2		6.73	N/A^5	
SRP 100-2	Load	10.03	6.59	42.87	46.33	N/A^4	59.77	66.11	N/A^4
	Defl.	1.01	0.17^2	8.3	2.68^2		6.48	N/A^5	
SRP U100	Load	15.59	6.59	52.68	46.33	2489	68.83	66.11	4068
	Defl.	0.65	0.17^2	3.93	2.68^2		9.44	N/A^5	

[1]: the yield load was obtained when ε_s reached 0.00236 ($\varepsilon_s = f_y / E_s$)

[2]: the theoretical deflection was obtained based on ACI 318-02 Cl. 9.5.2.2, accounting for SRP in transformed section analysis

[3]: the mid-span strains on the SRP sheet were measured using strain gauges

[4]: the strain gauge at mid-span malfunctioned

[5]: theoretical deflections at ultimate were not calculated
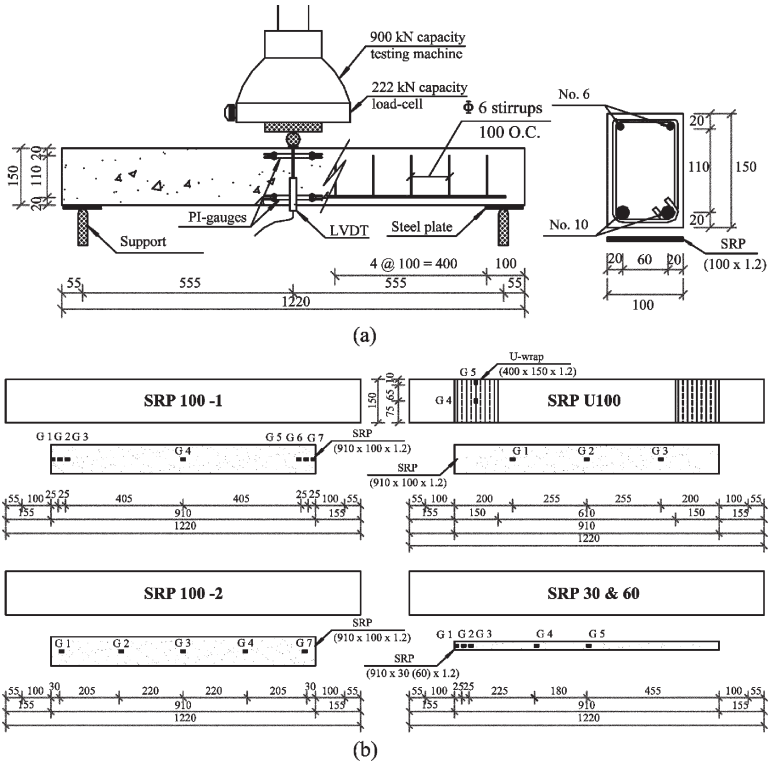
Figure 1 — Details of test beams: (a) test set-up and typical beam details;
(b) SRP strengthening schemes and strain gauge locations
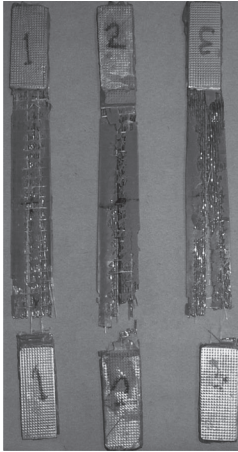
(a)   (b)
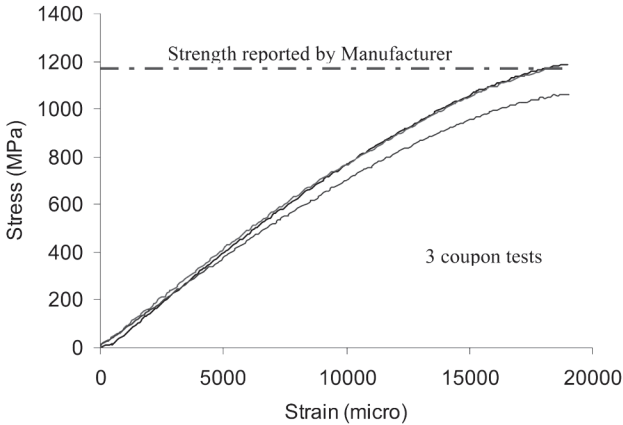
(c)

Figure 2 — Results of SRP coupon tests: (a) coupon test set-up; (b) coupons after failure; (c) stress-strain responses
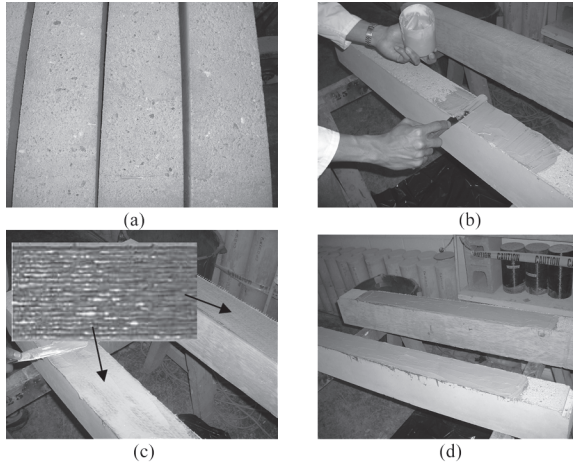
Figure 3 – Typical application procedure of SRP: (a) sandblasted concrete surface; (b) resin applied; (c) Hardwire® impregnated; (d) additional resin applied
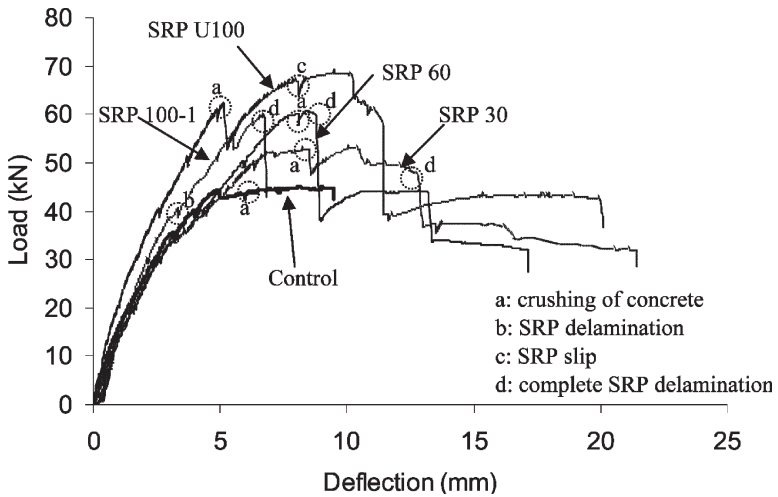
Figure 4 — Flexural response of test beams
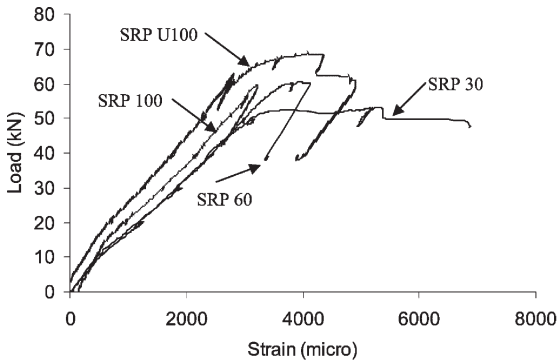
(a)
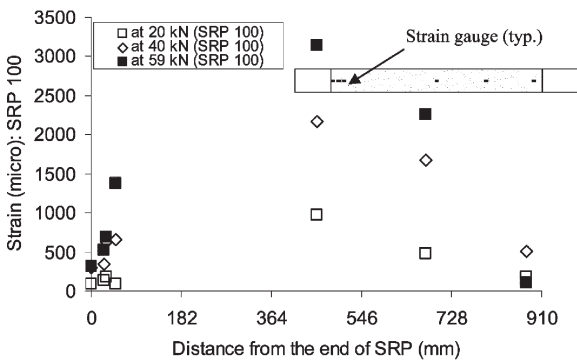
(b)

Figure 5 – SRP strains at various load levels: (a) load vs. mid-span SRP strains; (b) typical strain distribution along the SRP sheet (SRP 100)
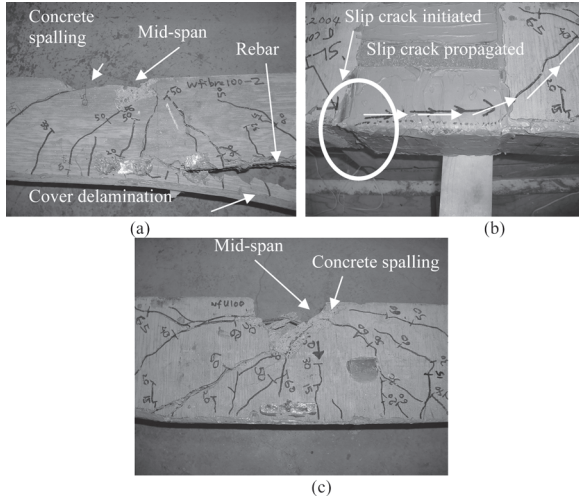
Figure 6 – Failure modes and crack patterns of test specimens: (a) delamination and crack pattern in SRP 100; (b) slip-failure at the end of SRP in SRP U100; and (c) crack pattern of SRP U100 at mid-span
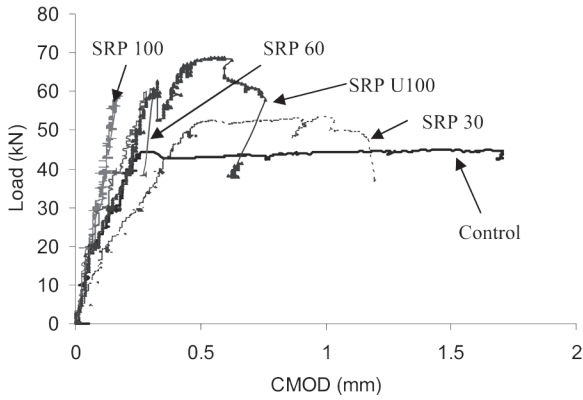

Figure 7 – Comparison of the crack mouth opening displacements
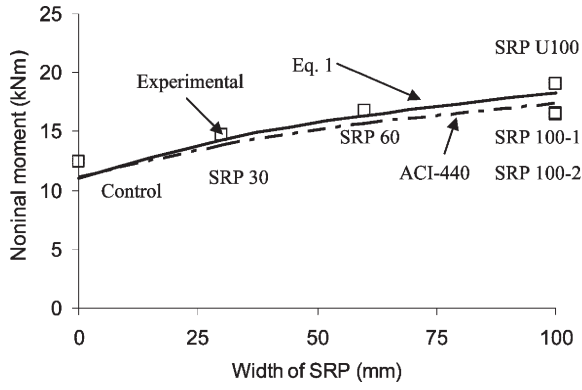
Figure 8 – Effect of width of SRP sheet on nominal moment capacity
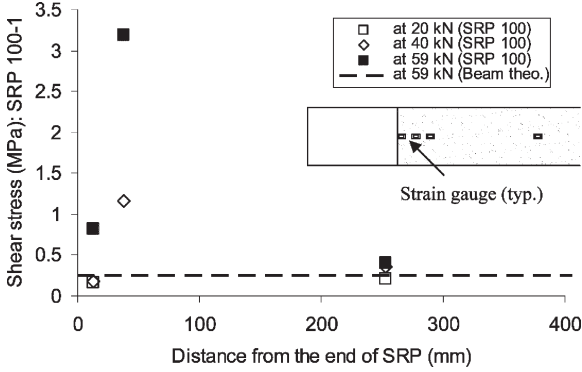
Figure 9 – Shear stress distributions near the cut-off point (SRP 100)